The International Archives of the Photogrammetry, Remote Sensing and Spatial Information Sciences, Volume XLVIII-1/W6-2025
3rd International Workshop on Evaluation and BENCHmarking of Sensors, Systems and
GEOspatial Data in Photogrammetry and Remote Sensing (GEOBENCH), 20–21 November 2025, Wroclaw, Poland

Analysis of morphological changes under controlled environmental conditions using UAV image-based bathymetry in very shallow waters

Paulina Kujawa [1], Jaroslaw Wajs [1], Damian Kasza [1]

[1] Department of Geodesy and Geoinformatics, Wrocław University of Science and Technology, Wrocław, Poland - (paulina.kujawa, jaroslaw.wajs, damian.kasza)@pwr.edu.pl

Keywords: Bathymetry, Photogrammetry, Morphological changes, Deposition, Erosion.

Abstract

Coastal environments present a challenge to traditional hydroacoustic methods (e.g. echo sounders) primarily due to their very shallow depth. Therefore, fast and effective methods of reconstructing the seafloor morphology are needed. This study aimed to evaluate the accuracy, uncertainty and reliability of the proposed UAV–SfM-based processing with geometric refraction correction for detecting morphological changes in a controlled shallow-water environment. The analysis focused on the impact of flight altitude (12 m and 61 m), water surface modelling and uncertainty propagation on classifying erosion, accumulation and non-change zones. Four UAV data acquisition campaigns were conducted. Total uncertainty was defined as a combination of instrumental errors, photogrammetric model accuracy, and water surface determination accuracy. Based on this, the LoD_{95} thresholds used for change detection with the M3C2 method were calculated. The obtained LoD_{95} values confirmed that changes exceeding ~2–3 cm can be reliably detected. The classification consistency between data sets obtained from low and high flight height reached an average overall accuracy of 77%, proving the stability and robustness of the developed process. These results demonstrate the efficiency and repeatability of the proposed workflow, which allows for the quantitative assessment of morphological changes in controlled shallow water conditions, with potential applications in similar natural environments.

1. Introduction

It is estimated that around 30–40% of the global population lives in coastal areas (up to 50 km from shore), highlighting the importance of understanding geological processes in these regions. Coastal environments undergo frequent and dynamic changes caused by waves, tides and currents. Changes in seafloor morphology are particularly evident after extreme events such as storms or tsunamis. Monitoring these areas for changes such as erosion and deposition is crucial for effective management and ensuring navigation safety, as well as for assessing the risks associated with extreme phenomena.

Traditional techniques for mapping marine areas include the use of single- and multi-beam echo sounders, as well as sonars. However, due to depth measurement limitations, alternative methods such as image- and LiDAR-based bathymetry are increasingly being used for shallow water areas (Kujawa & Remondino, 2025). These sensors are usually mounted on aerial, airborne or satellite platforms. However, due to cost and time efficiency considerations, drone-based imaging has emerged as a more optimal solution.

Monitoring coastal areas with passive sensors is feasible under certain conditions. Primarily, the water must be sufficiently clear, with the seafloor visible. Additionally, it is advisable to capture images during calm weather conditions, particularly when the water surface is undisturbed by wind. Finally, the position of the sun should be near the horizon to minimize the effects of sun glints in the images.

One of the main challenges in processing photogrammetric data for underwater applications is refraction correction. A wide range of methods have been developed in the literature, including geometric approaches (Dietrich, 2017), integrated radiometric-geometric techniques (Slocum et al., 2020), and deep learning-based methods (Agrafiotis & Demir, 2025).

Provided that uncertainties are verified and corrected, the resulting 3D model of the seafloor can accurately reflect its actual morphology. This enables the model to be used for further geomorphological and environmental analyses. Popular applications of these models include detecting erosional and depositional patterns (Alevizos & Alexakis, 2022), monitoring the evolution of nearshore sandbars (Alevizos, 2024) and mapping coastal habitats (Ventura et al., 2023).

The detection of morphological changes mainly focuses on land areas. In the study by Pucino et al. (2021), the authors analysed the dynamics of changes in open and bay beaches using quantitative volume and profile analysis methods. They also developed a set of indicators to assess beach topography dynamics. Another study, by Brunetta et al. (2021), discussed the use of drones in coastal wetlands. The researchers examined morphological changes in tidal flats and assessed the accuracy of Digital Surface Models (DSMs) used in morphodynamic analyses. Leisner et al. (2024) used the M3C2 (Multiscale Model-to-Model Cloud Comparison) algorithm to analyse changes to the coastal landscape and estimate volume changes based on digital surface models.

Researchers have also addressed the topic of quantifying geomorphological changes in underwater areas. In the paper by Woodget et al. (2019), the authors emphasised that such changes can be detected with a level of accuracy comparable to that achieved in terrestrial environments, without the need for different approaches. He et al. (2021) compared digital elevation models by creating difference models (DoDs) to evaluate changes in lake topography before and after an earthquake. In summary, a wide range of analytical methods are employed to evaluate morphological changes in topographic and shallow-water environments. Differential models are the most common method of quantitatively determining sediment changes over time, although point cloud comparison, including the M3C2 method, is also becoming more popular.

The results obtained from data processing are subject to measurement uncertainties, and accounting for these errors allows for a more reliable characterization of the analyzed topography. In the study by Duo et al. (2021), the researchers investigated short-term changes in artificial dunes. In their analysis, they considered the change detection threshold (TCD), which was approximately 0.15 m. This enabled them to distinguish between actual morphological changes and changes resulting from the uncertainty of the elevation data. Another study, by Woodget et al. (2019), focused on analysing measurement uncertainties associated with the reconstruction of submerged topography in coastal areas. The authors modelled errors in DEM accuracy obtained using machine learning, based on the relationships between error and independent variables such as water surface elevation, terrain slope, vegetation, surface roughness, measurement point density and image sharpness. They also demonstrated that improving estimates of water surface elevation is essential for accurately mapping underwater topography, reducing mean elevation error by up to 73% and standard deviation by up to 69%.

This study, which was conducted under controlled marine conditions, aimed to evaluate the effectiveness of using UAV photogrammetry to detect morphological changes in shallow waters. The study examined how drone flight altitude (12 m or 61 m) impacted the accuracy of bathymetric reconstruction and the effectiveness of refraction correction. The ability to detect morphological changes in the coastal zone was also investigated. Specifically, the extent to which various acquisition parameters (e.g. flight altitude and Ground Sampling Distance (GSD)) and environmental conditions affect the accuracy of depth models, the uncertainty of water surface determination, and the quality of seafloor change classification was analysed. As part of the research, results obtained for pairs of scenarios with different flight heights were compared; the LoD_{95} threshold for detecting changes was determined; and the consistency of erosion, accumulation and no-change zone classifications was assessed.

2. Study area and dataset

The experiment was performed in a finite-sized water reservoir with dimensions 7.3 m × 3.7 m and a maximum depth of 1 m. It replicates the shallow water of a coastal area (see Figure 1). The bottom of the tank is composed of river sand and rocks (aggregate). The water is highly transparent, ensuring full visibility of the bottom. The water depth is maintained at approximately 0.8 m

Figure 1. A study site with a pool simulating shallow waters.

The UAV photogrammetric survey was taken using DJI Mavic 3M drone equipped with a RGB camera. Images were captured from a nadir position at heights of approx. 12 m and 61 m, at a flight speed of 2 m/s. The sensor records images with a resolution of 20 MP and a size of 5280 x 3956 pixels, with a focal length of 12.29 mm. Measurements were conducted for five scenarios simulating morphological changes, taking into account both erosion and sedimentation processes. The tank bottom morphology was modified by controlled addition or removal of material (sand and aggregate).

Six ground control points (GCPs), which were located around the pool, and two check points (CPs) (i.e. underwater points inside the facility), were used to assign georeferences. GCPs were measured with a total station, achieving 5″ angular accuracy and 2 mm + 2 ppm in distance. CPs were acquired using GNSS RTK with a Leica GS18 T, delivering single-baseline accuracies of 8 mm + 1 ppm horizontally and 15 mm + 1 ppm vertically. Water depth was measured independently at several locations within the reservoir to calculate the average water level. The depth of the points was estimated using a linear measure with an accuracy of about 3 mm. In addition, two longitudinal profiles were captured during each measurement series.

3. Methods

The methodology for acquiring and processing data on the underwater area in order to detect morphological changes is shown in Figure 2.

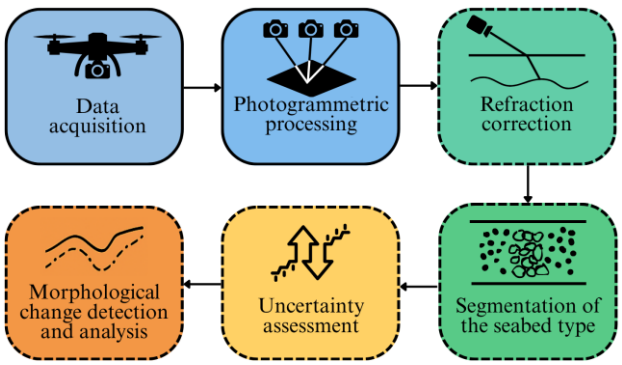

Figure 2. Graphical schema of data acquisition and processing.

The RGB imagery obtained from the UAV survey was subjected to photogrammetric processing in accordance with standard procedures, including: (i) identification and introduction of GCPs and CPs; (ii) image orientation; (iii) generation of sparse and dense point clouds; (iv) orthomosaic creation.

Next, the *pyBathySfM* geometric approach (Dietrich, 2019) proposed by Dietrich (2017) was used to perform refraction correction. This method was tested by the authors, among others, in the work of Kujawa et al. (2025), achieving an accuracy of 3-5 centimetres (average value based on echo-sounder data and GNSS measurements) at an average depth of approx. 1.2 m.

An additional step was taken - the area was manually divided into segments based on the created orthomosaics. This allowed the distinction between sandy and rocky zones, improving the interpretation and understanding of morphological changes.

The final step in the proposed methodology was change detection. Before morphological changes can be classified as erosion, deposition or no change, a level of detection (LoD) should be determined to define value classes. As each scenario's product is subject to uncertainty, errors between epochs are propagated. For each pair of epochs, the two-sided 95% LoD (Lague et al., 2013) is:

$$LoD_{95} = 1.96\sqrt{\sigma_{z,i}^2 + \sigma_{z,i+1}^2} \quad (1)$$

A separate registration term was not included because all epochs were solved in the same global reference frame and co-registered on stable ground.

The uncertainty for each epoch is distributed as follows:

$$\sigma_{z,i} = \sqrt{\sigma_{SfM,z,i}^2 + \sigma_{WS,i}^2 \left(+\sigma_{ref,i}^2\right)\left(+\sigma_{env,i}^2\right)} \quad (2)$$

where:
$\sigma_{SfM,z,i}$ - vertical uncertainty from the photogrammetric processing,
$\sigma_{WS,i}$ - uncertainty of the mean water surface used for refraction correction,
$\sigma_{ref,i}$ - refractive-index (n) uncertainty,
$\sigma_{env,i}$- optional environmental factors (e.g., turbidity, waves, sun glint).

The GCP RMSE Z value was used to calculate the photogrammetric processing error. The uncertainty of the water surface was assessed from the instrumental errors and the number of points used to estimate the mean water level:

$$\sigma_{WS,i} = \sqrt{\frac{\sigma_{GNSS}^2 + \sigma_{depth}^2}{n}} \quad (3)$$

where:
σ_{GNSS} - the vertical GNSS error for the bottom point,
σ_{depth} - the accuracy of the depth measurement,
The uncertainty of refraction correction ($\sigma_{ref,i}$) was omitted due to the negligible impact of refraction error in very shallow water. Environmental uncertainty ($\sigma_{env,i}$) was disregarded as well because the water was clear, with no sun glints or surface chop.

Finally, the classification was as follows:
- deposition: $\Delta z > LoD_{95}$,
- no change: $\Delta z \leq LoD_{95}$ and $\Delta z > -LoD_{95}$,
- erosion: $\Delta z < -LoD_{95}$.

Morphological changes (Δz) were determined by comparing two point clouds using the M3C2 algorithm. The algorithm works directly on point clouds, eliminating the need to create a mesh or grid. It calculates the local distance between two point clouds along the surface's normal direction and tracks changes in surface orientation in 3D. Depending on the roughness of the point clouds and the registration error, the algorithm estimates a confidence interval for each distance measurement (Lague et al., 2013).

In the final stage, seafloor cross-sections were extracted along fixed transects for both survey periods. This enabled clear visualisation of elevation changes and supported the interpretation of key morphodynamic processes.

4. Results

Photogrammetric processing was performed in Agisoft Metashape Professional, version 2.2.1. Localization of each GCP is shown in Figure 3. The quality metrics are summarised in Table 1. There is a noticeable variation in RMSE values between scenarios, probably due to differences in environmental conditions during data collection. Although the measurements were performed in a repeatable manner using the same methodology and equipment, some days were cloudy while on others there were local sun glints on the water's surface. As the control points were located in the reservoir, their position in the images was subject to refractive error and variable lighting conditions. For this reason, and due to the difficulty in clearly determining the depth of the control points, the Z component was not included in the accuracy assessment.

Figure 3. The study site with the location of the GCPs, CPs and profile's points.

Scenario No.	Flight height [m]	Number of images	GSD [mm/ pix]	GCPs XYZ RMSE [mm]	CPs XY RMSE [mm]
1a	12.4	100	3	5	13
1b	61.3	16	16	8	13
2a	12.4	100	3	14	14
2b	61.2	16	16	10	16
3a	12.4	93	3	10	15
3b	61.2	16	16	11	15
4a	12.5	104	3	9	15
4b	61.4	16	16	10	14

Table 1. Key quality metrics for photogrammetric processing.

For each scenario (1, 2, 3, 4), the water level was determined by adding the measured depth to several underwater points obtained using the GNSS RTK technique and then averaging their values. The standard deviations of the calculated water levels ranged from 2 to 6 mm. This confirms that water levels remained stable throughout all periods. The lowest standard deviation (2 mm) was obtained in scenario 2, where the water level was calculated based on five points with very similar values. The highest deviation (6 mm) occurred in epoch 4, potentially due to the lower accuracy of the ruler measurement.

Refraction correction followed the geometric *pyBathySfM* approach of Dietrich (2017, 2019). A separate true depth is determined for each refraction angle, and the average of all the results is considered the most reliable. To minimise errors, the calculations included only data where the refraction angle was less than 35 degrees from the nadir, as in the work of Woodget et. al. (2019). Table 2 presents the corrected depth statistics obtained at different epochs. Each pair of scenarios (1a–1b, 2a–2b, 3a–3b, and 4a–4b) presents data collected during the same acquisition under identical water level conditions, differing only in flight altitude. The corrected depth ranges are similar in each pair. The average depth values differ by no more than 19 mm, and the maximum depth differences are less than 21 mm. However, differences in minimum depths, in some cases reaching 84 mm, are likely due to differences in the coverage area of the reservoir or less image overlap at higher flight altitudes.

Scenario No.	Min depth [m]	Mean depth [m]	Max depth [m]
1a	0.544	0.791	0.900
1b	0.550	0.783	0.879
2a	0.447	0.789	0.901
2b	0.363	0.770	0.897
3a	0.520	0.787	0.936
3b	0.545	0.781	0.878
4a	0.520	0.781	0.934
4b	0.538	0.789	0.917

Table 2. A summary of the corrected depth ranges for different scenarios.

The corrected point clouds were then compared with the GNSS-measured profiles (included in Figure 3). The results of this comparison are shown in Table 3. An accuracy assessment based on bottom profiles revealed a negative ΔZ following refraction correction, with respective averages of −20 mm and −32 mm for low and high flights, and standard deviations of 11 mm and 27 mm, respectively. For each pair (a and b), the flight at a higher altitude resulted in a more negative bias and greater dispersion. This can be attributed to the influence of a greater GSD and lower reconstruction precision. The best fit was obtained in scenario 2a, with an average bias of −11 mm and a standard deviation of 7 mm. The largest dispersion was observed in scenario 3b, with an average bias of −38 mm and a standard deviation of 38 mm.

Scena-rio No.	Flight height [m]	No. of points	Mean	Median	Std. dev.
			vertical difference ΔZ [mm]		
1a	12.4	17	-13	-12	11
1b	61.3	10	-24	-22	22
2a	12.4	29	-11	-9	7
2b	61.2	23	-34	-32	21
3a	12.4	26	-28	-27	12
3b	61.2	25	-38	-34	38
4a	12.5	25	-28	-24	13
4b	61.4	25	-31	-25	28

Table 3. Assessment of the accuracy of refraction-corrected point clouds using bottom profiles.

In the next stage, the LoD_{95} was calculated for each pair of epochs and used as the threshold to classify morphological changes. The results obtained for the uncertainties are presented in Table 4. Morphological changes were analysed using the M3C2 method to compare scenarios with different flight altitudes. The results of the identified zones of erosion, no changes and deposition are shown in Figure 4. The photogrammetric uncertainty values ($\sigma_{SfM,z}$) and water surface model error values ($\sigma_{WS,i}$) for each scenario range from 3 to 11 mm, confirming the high quality of the reconstruction. The LoD_{95} values determined for the compared pairs of scenarios range from 25 to 35 mm. Lower thresholds (25–27 mm) were obtained for flights at lower altitudes (scenarios a), while higher thresholds (32–35 mm) were observed for flights at higher altitudes (scenarios b). This suggests that the model's accuracy and capacity to detect subtle morphological changes decrease with increasing flight altitude. This is consistent with the discrepancies observed in the accuracy of control points and the outcomes of bottom profile comparisons.

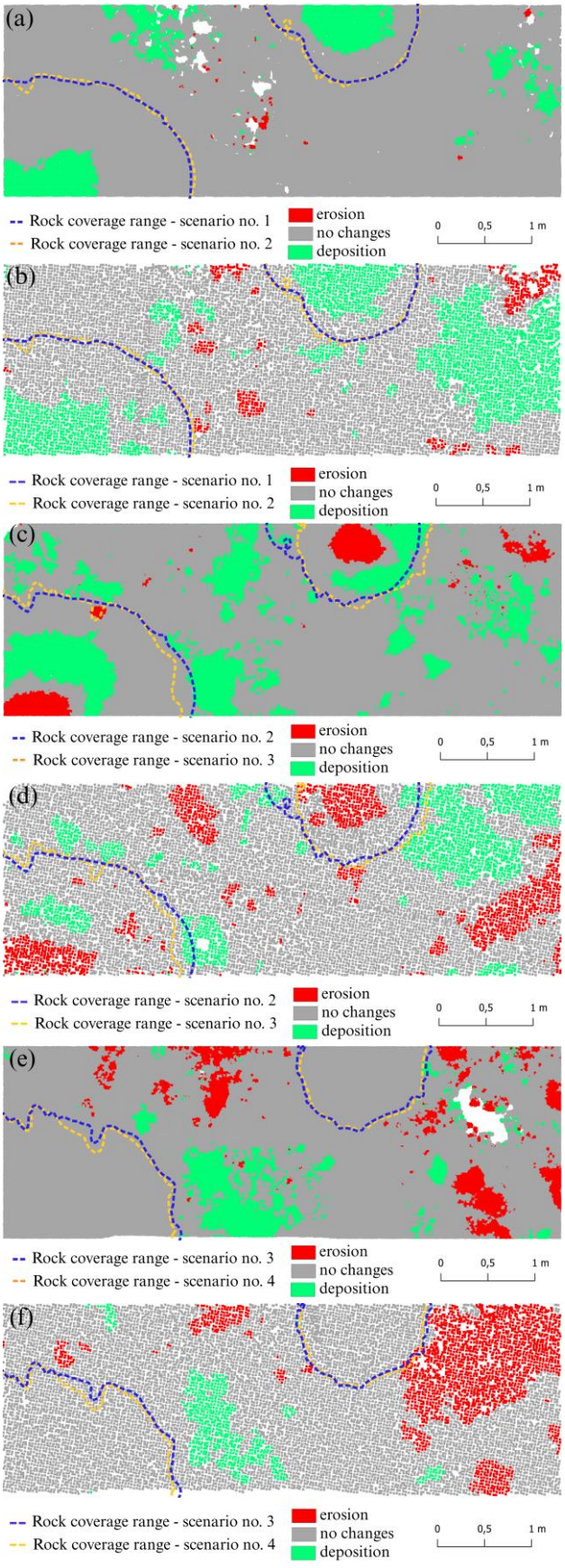

Figure 4. Morphological change detection between scenarios: (a) no. 1a and 2a; (b) no. 1b and 2b; (c) no. 2a and 3a; (d) no. 2b and 3b; (e) no. 3a and 4a; (f) no. 3b and 4b.

Comparison	$\sigma_{SfM,z1}$ [mm]	$\sigma_{SfM,z2}$ [mm]	σ_{WS1} [mm]	σ_{WS2} [mm]	σ_{z1} [mm]	σ_{z2} [mm]	LoD_{95} [mm]
1a-2a	3	8	11	8	12	11	32
1b-2b	7	9	11	8	13	12	35
2a-3a	8	4	8	7	11	8	27
2b-3b	9	11	8	7	12	13	35
3a-4a	4	7	7	8	8	10	25
3b-4b	11	8	7	8	13	11	34

Table 4. Key quality metrics for photogrammetric processing.

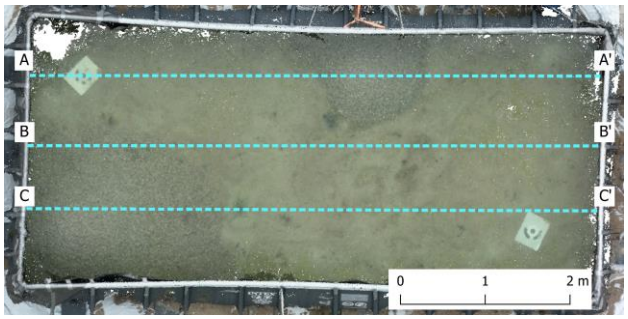

Figure 5. Map of location cross-sections for morphological changes detection.

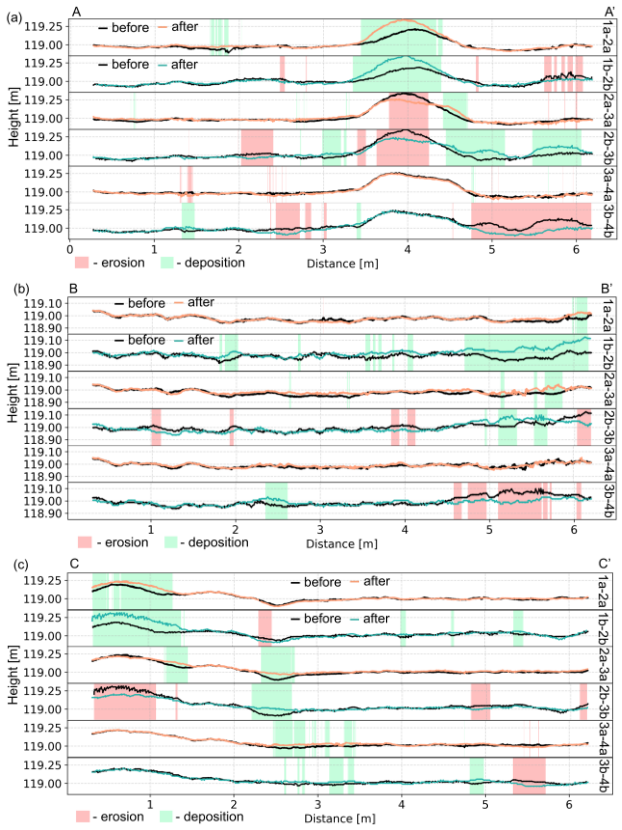

Figure 6. Cross-sections: (a) A-A'; (b) B-B'; (c) C-C'.

Another product used to detect morphological changes was a set of bottom surface cross-sections, which provided a more detailed insight into the dynamics of change. Figure 5 shows the spatial distribution of the cross-sections, while Figure 6 presents the cross-sections generated for each pair of epochs, grouped according to the flight altitude of the UAV. Comparing sets a and b between individual scenarios shows that the detectability of erosion and accumulation zones in aggregate areas is consistent in both cases. However, differences appear in sandy areas, where greater discrepancies in the classification of morphological changes were observed.

5. Discussion

Image-based UAV bathymetry can only be used when the water is clear enough to see the seafloor. Figure 7 shows an area affected by turbidity that could not be reconstructed during processing. For comparison, an area of clear water and its corresponding reconstruction are also shown. It is important to emphasise the limitations of this method.

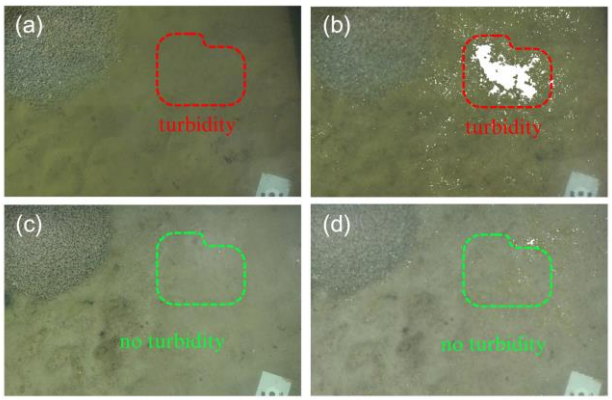

Figure 7. Turbidity analysis showing UAV-acquired images (a, c) and their corresponding orthomosaic views (b, d).

One of the most important issues in the proposed processing method is the reliable determination of the area of the water surface. Various methods are employed in practice, ranging from shoreline-based estimation and point measurement of the seafloor with depth readings to determining the water level based on a photogrammetric model or other technologies, such as LiDAR. Due to the focus of the methodology on time and cost efficiency, and the absence of a natural shoreline at the analysed facility, the point method (GNSS RTK + depth) was employed, based on an average of 2–5 points per scenario. Standard deviations of the water level of 2–6 mm were obtained, confirming the stability of the conditions during measurement and enabling reliable refraction correction. However, this method assumes a uniform water level. Therefore, if there is a risk of inclination, it is recommended that the number of points be increased and the water level plane be adjusted.

Refraction correction is an important step in processing image-based bathymetric data, providing the actual depth of the reservoir bed. While the scientific literature describes various approaches, this study opted for a well-established geometric method, which allows for fast and efficient processing without the need for advanced statistical calculations. The obtained depth values were compared with GNSS point measurements, resulting in average errors ranging from 11 to 38 mm and a standard deviation ranging from 7 to 38 mm at an average depth of approximately 0.8 m. Considering the accuracy of the GNSS instrument (15 mm + 1 ppm vertically) and other sources of uncertainty, these results are very good and fully acceptable for UAV bathymetry in shallow waters.

Measurement uncertainties are a key element in the processing that determines thresholds (LoD_{95}) for classifying erosion, deposition and no change. The studies primarily considered instrumental and photogrammetric processing errors, as well as the uncertainty of the water surface model. These errors were

then propagated to the LoD_{95} values. Errors with little impact, such as refraction errors, were omitted.

The resulting classes of morphological change were used to compare pairs of scenarios and are presented in map form. The visual results are consistent with the assumed morphological manipulations and accuracy analyses:
(i) Epochs 1–2: only simulated accumulation was applied between these epochs. The maps show sedimentation zones dominating, with only occasional erosion zones. This may be the result of sand surface reconstruction, for example due to high sand surface roughness, limited contrast or turbidity.
(ii) Epochs 2 and 3: erosion and deposition simulations were applied to both types of substrate. The maps show the presence of these processes.
(iii) Epochs 3–4: During this period, only sand sedimentation and erosion processes were applied. Changes are concentrated in sandy areas, while rocky areas remain unchanged.

The analysis of point classification consistency, presented in Table 5 for the erosion, no change and deposition classes, demonstrated an average overall accuracy of 77% across the three analysed comparisons. This indicates a high degree of consistency between classifications obtained from UAV data acquired at 12 m and 61 m heights. Consistent results across different flight heights confirm the effectiveness of the proposed workflow combined with change detection thresholds based on the LoD_{95} value in reducing the impact of measurement uncertainties on morphological change detection results. However, it should be emphasised that local discrepancies mainly occurred in sandy areas where the homogeneous surface texture and increased water turbidity limited visibility of the seafloor. Such phenomena may affect the accuracy of photogrammetric reconstruction and lead to incorrect classification of changes. Despite these local differences, the overall level of agreement confirms the reliability of the approach used.

Scenarios	Matched points	Overall accuracy
1a&2a vs 1b&2b	308,479 / 309,479	77.3%
2a&3a vs 2b&3b	306,253 / 308,104	71.3%
3a&4a vs 3b&4b	299,558 / 314,664	81.7%

Table 5. Consistency of morphological process classification between low- and high-altitude UAV datasets.

6. Conclusions

The research confirmed that the proposed methodology for processing UAV data for bathymetric purposes can detect quantitative morphological changes in shallow waters. The obtained LoD_{95} values show that the method can detect changes of more than 2–3 cm while producing consistent results from data collected at different flight altitudes. Local discrepancies identified in sandy areas result from their homogeneous texture and increased water turbidity, both of which impact the accuracy of photogrammetric reconstruction. The proposed workflow is repeatable and scalable, and could be used to monitor the morphodynamics of shallow coastal environments.

Future research will focus on implementing the developed methodology to real-world objects such as coastal zones or calm river areas.

References

Agrafiotis, P., & Demir, B. 2025. Deep learning-based bathymetry retrieval without in-situ depths using remote sensing imagery and SfM-MVS DSMs with data gaps. *ISPRS Journal of Photogrammetry and Remote Sensing*, 225, 341–361. https://doi.org/10.1016/j.isprsjprs.2025.04.020

Alevizos, E. 2024. Quantification of Nearshore Sandbar Seasonal Evolution Based on Drone Pseudo-Bathymetry Time-Lapse Data. *Remote Sensing*, 16(23), 4551. https://doi.org/10.3390/rs16234551

Alevizos, E., & Alexakis, D. D. 2022. Monitoring Short-Term Morphobathymetric Change of Nearshore Seafloor Using Drone-Based Multispectral Imagery. *Remote Sensing*, 14(23), 6035. https://doi.org/10.3390/rs14236035

Brunetta, R., Duo, E., & Ciavola, P. 2021. Evaluating Short-Term Tidal Flat Evolution Through UAV Surveys: A Case Study in the Po Delta (Italy). *Remote Sensing*, 13(12), 2322. https://doi.org/10.3390/rs13122322

Dietrich, J. T. 2017. Bathymetric structure-from-motion: Extracting shallow stream bathymetry from multi-view stereo photogrammetry. *Earth Surface Processes and Landforms*, 42(2), 355-364. https://doi.org/10.1002/esp.4060

Dietrich, J. T. 2019. pyBathySfM v4.0 (v4.0). Zenodo. https://doi.org/10.5281/zenodo.3377602

Duo, E., Fabbri, S., Grottoli, E., & Ciavola, P. 2021. Uncertainty of Drone-Derived DEMs and Significance of Detected Morphodynamics in Artificially Scraped Dunes. *Remote Sensing*, 13(9), 1823. https://doi.org/10.3390/rs13091823

He, J., Lin, J., Ma, M., & Liao, X. 2021. Mapping topo-bathymetry of transparent tufa lakes using UAV-based photogrammetry and RGB imagery. *Geomorphology*, 389, 107832. https://doi.org/10.1016/j.geomorph.2021.107832

Kujawa, P., & Remondino, F. 2025. A Review of Image- and LiDAR-Based Mapping of Shallow Water Scenarios. *Remote Sensing*, 17 (12), 2086. https://doi.org/10.3390/rs17122086

Kujawa, P., Wajs, J., & Pleśniak, K. 2025. The approach to UAV image acquisition and processing for very shallow water mapping. *International Journal of Applied Earth Observation and Geoinformation*, 141, 104604. https://doi.org/10.1016/j.jag.2025.104604

Lague, D., Brodu, N., & Leroux, J. (2013). Accurate 3D comparison of complex topography with terrestrial laser scanner: Application to the Rangitikei canyon (N-Z). ISPRS Journal of Photogrammetry and Remote Sensing, 82, 10–26. https://doi.org/10.1016/j.isprsjprs.2013.04.009

Leisner, M., de Paula, D. P., Albuquerque, M. da G., Façanha, M. C., Vasconcelos, Y. G., & de Morais, J. O. 2024. Applications of UAV-SfM Remote Sensing in Monitoring Morphodynamic Processes in Sedimentary Cliffs of Pacheco Beach, Northeast Brazil. *Journal of Coastal Research*, 113(sp1). https://doi.org/10.2112/jcr-si113-110.1

Pucino, N., Kennedy, D. M., Carvalho, R. C., Allan, B., & Ierodiaconou, D. 2021. Citizen science for monitoring seasonal-

scale beach erosion and behaviour with aerial drones. *Scientific Reports*, 11(1). https://doi.org/10.1038/s41598-021-83477-6

Slocum, R. K., Parrish, C. E., & Simpson, C. H. 2020. Combined geometric-radiometric and neural network approach to shallow bathymetric mapping with UAS imagery. *ISPRS Journal of Photogrammetry and Remote Sensing*, 169, 351–363. https://doi.org/10.1016/j.isprsjprs.2020.09.002

Ventura, D., Grosso, L., Pensa, D., Casoli, E., Mancini, G., Valente, T., Scardi, M., & Rakaj, A. 2023. Coastal benthic habitat mapping and monitoring by integrating aerial and water surface low-cost drones. *Frontiers in Marine Science*, 9. https://doi.org/10.3389/fmars.2022.1096594

Woodget, A. S., Dietrich, J. T., & Wilson, R. T. 2019. Quantifying Below-Water Fluvial Geomorphic Change: The Implications of Refraction Correction, Water Surface Elevations, and Spatially Variable Error. *Remote Sensing*, 11(20), 2415. https://doi.org/10.3390/rs11202415

Acknowledgements

The work was supported by the project Minigrants for doctoral students of the Wroclaw University of Science and Technology.